Rare Metal Materials and Engineering
Volume 49, Issue 11, November 2020
Available online at www.rmme.ac.cn

Science Press

Cite this article as: Rare Metal Materials and Engineering, 2020, 49(11): 3796-3802.

ARTICLE

Research on Phases and Morphology of Sm_2Fe_{17} Melt-Spun Ribbon

Liu Kun[1], Wang Shuhuan[1,2], Feng Yunli[1], Zhang Yikun[1]

[1] College of Metallurgy and Energy, North China University of Science and Technology, Tangshan 063210, China; [2] Tangshan Key Laboratory of Special Metallurgy and Material Manufacture，Tangshan 063210, China

Abstract: The effects of the quenching speed on the phase composition and morphology of the Sm-Fe alloy ribbons were analyzed by X-ray diffraction (XRD), optical microscope (OM), scanning electron microscope (SEM) and high-resolution transmission electron microscope (HRTEM). With the increase of wheel speed, the size of alloy ribbons decreased along the width and thickness direction firstly, and that existed stably in the thickness direction even when the speed increased sequentially. The size of agglomeration decreased in the free surface, which was 0.5~3 μm when the quenching speed was increased up to 36 m/s. The XRD and EDS results show that there are three different phases in the ribbons: Sm_2Fe_{17}, α-Fe and Sm-rich phase. The grain size of Sm_2Fe_{17} phase in the ribbons is on the sub-micron scale (d_m≈340 nm, 36 m/s), which is restricted not only by the wheel speed but also by the bare number of elements.

Key words: grain morphology; wheel speed; grain agglomeration; Sm-Fe alloy

The research for magnetic materials has extended to the frontiers of physics and material science, etc. With the advantages of high-energy-product Nd-Fe-B permanent magnets, the research and development of permanent magnetic materials have been mainly concentrated on the alloys with rare earths[1-3]. Among all kinds permanent magnetic materials, the Sm-Fe based alloys, such as the Th_2Zn_{17}-type $Sm_2Fe_{17}N_x$[4,5], $ThMn_{12}$-type $SmFe_{11}Ti$[6,7] and $TbCu_7$-type $SmFe_9N_x$[8-10], have been considered as the potential materials for the application of permanent magnet. One achievement of these efforts was the discovery of the $Sm_2Fe_{17}N_x$ intermetallic compound with a rhombohedral Th_2Zn_{17}-type structure. With a high Curie temperature, $Sm_2Fe_{17}N_x$ intermetallic compound can meet the requirement for permanent magnet when applied in high temperature environment (engine, servo motor, wind power generation, etc)[11,12]. Permanent magnetic material researchers mainly focused on the studies of magnetic detection and analysis of permanent magnetic material with different adding elements[13-16], preparation methods[17-20] and nitridation conditions[21,22]. Rare attention was paid in the formation mechanism of morphology and microstructure of Sm-Fe alloy ribbon synthetically. To improve the magnetic properties and squareness, we aim for in-depth research of the microstructure and grain size, which has been studied widely but not synthetically. We all know that the key process to obtain perfect magnetic properties is to control the microstructure before nitridation process.

This research mainly investigated the phase composition and morphology of the Sm_2Fe_{17} melt-spun ribbons in greater detail by combining OM, XRD, SEM, and HRTEM characterization methods synthetically, which can offer a help to the follow-up studies.

1 Experiment

Master alloys composed of Sm_2Fe_{17} were prepared by induction melting Sm (99.95 wt%) and Fe (99.95 wt%) in Ar gas atmosphere. An extra amount of 5 wt% Sm was added to compensate the mass losses during the processing. The molten were ejected in an orifice diameter of 0.6 mm at the bottom of a quartz crucible. All ribbons were prepared by ejection onto a rotating Cu-disk with the surface speeds

Received date: November 25, 2019
Foundation item: National Natural Science Foundation of China (51674123)
Corresponding author: Wang Shuhuan, Professor, North China University of Science and Technology, Tangshan 063210, P. R. China, E-mail: wshh88@ncst.edu.cn

of 12~45 m/s. The melt-spun ribbons were obtained as fragmented pieces (thickness: 18~30 μm; width: 1~3 mm). The XRD (Cu Kα, D8 ADVANCE) was used to determine the phases presented in the specimens. The microstructures of the ribbons were examined by a scanning electron microscope (SEM) equipped with an energy-dispersive X-ray spectroscopy (EDS) analyzer, and the morphology of phases was analyzed by TEM JEM-2100F, equipped with a cold cathode field-emission gun operated at the acceleration voltage of 200 kV. Specimens for TEM analysis were prepared by grinding the samples in an agate mortar with ethanol and depositing a few drops of the suspension on a Cu grid covered with a holey carbon layer.

2 Results and Discussion

Fig.1 shows that the size of ribbons in three-dimensional direction changes obviously with the increase of wheel speed. When the wheel speed is 12 m/s, the average size in width is 2~5 mm (shown in Fig.1a) and presents an elongated needle-shaped or crumb-shaped state as the wheel speed is up to 45 m/s (Fig.1c). It can be interpreted by the schematic diagram shown in Fig.2, adequately. The contact form of the drop and the rotating roller prompts the ribbons to be wedge-shaped along the rotation direction. Therefore, the fragmentation degree of ribbons is obvious when increasing the rotation speed. The size in both thickness and width directions decreases but showing an inevitably opposite trend in length direction due to the fragility of alloy itself.

OM measurement was performed to confirm the thickness variation of ribbons. Multiple statistical results in thickness direction are shown in Fig.3, and the section OM images are shown in Fig.4. The thickness shows a downward trend when increasing the wheel speeds. When the wheel speed is 12 m/s, the thickness is about 34 μm, as depicted in Fig.4a, and declines to an average thickness of ~19 μm when the wheel speed increases to 36 m/s (shown in Fig.4c). Increasing the wheel speed continuously has little effect on the thickness.

It can be concluded that the sizes of ribbons in three-dimensional directions are changed with the increase of wheel speed, which are declined slightly in width and thickness directions and broken severely in length direction. Taking the contact between individual droplets and the roll surface into consideration, the effective contact area is enhanced when increasing the wheel speed continuously. Droplets elongate along the rotating direction and result in the decrease of the size in width and thickness directions.

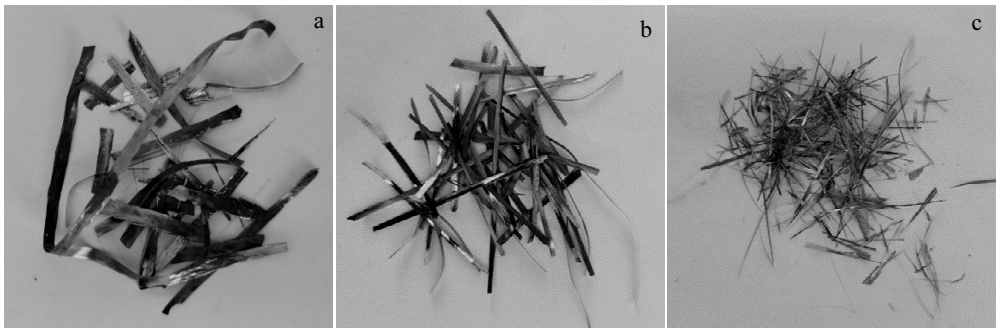

Fig.1 Sm-Fe ribbons at different wheel speeds: (a) 12 m/s, (b) 24 m/s, and (c) 45 m/s

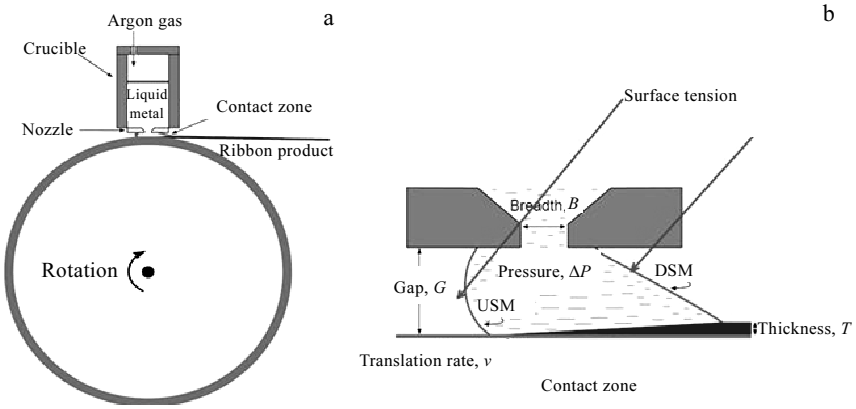

Fig.2 Schematic diagrams of melt-quenched process (a) and the contact surface of the drops and roller (b)

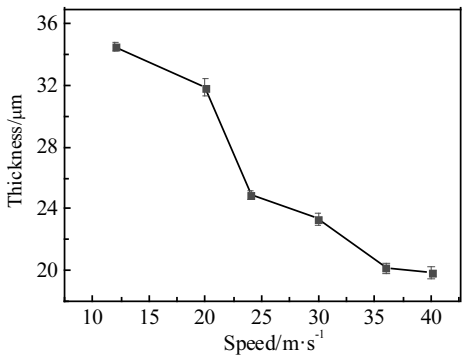

Fig.3 Change trend of thickness with the wheel speeds

As shown in Fig.5, the size of grain agglomeration is reduced with increasing the wheel speed. When the wheel speed is 12 m/s, the size is between 3.5~10 μm; $d_m \approx$ 6.03 μm, which represents the mean diameter, and it declines to $d_m \approx$ 3.0 μm when the wheel speed increases to 18 m/s, and the uniformity is improved to some extent. When the wheel speed is up to 36 m/s, the size decreases to ~1.96 μm, illustrating that the higher wheel speed is beneficial to the decrease of agglomeration size and the improvement of the uniformity.

Since the nucleation rate is greater than the growth rate, fine grains are obtained in the process of melt-spun process, resulting the increase of the surface atomic number and

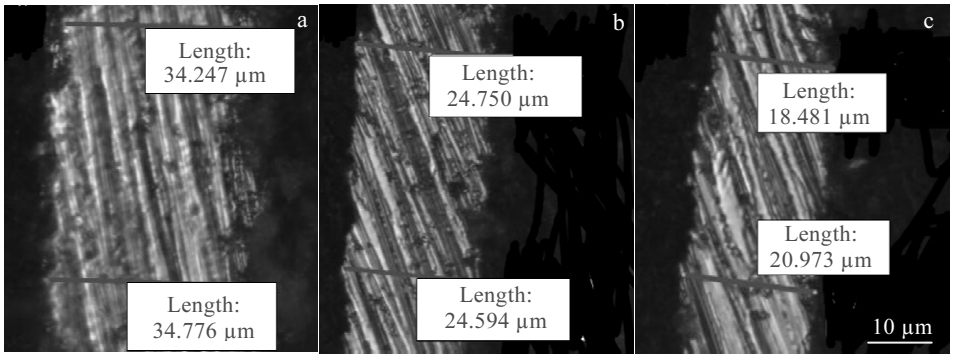

Fig.4 OM images of ribbons in the thickness direction at different wheel speeds: (a) 12 m/s, (b) 24 m/s, and (c) 36 m/s

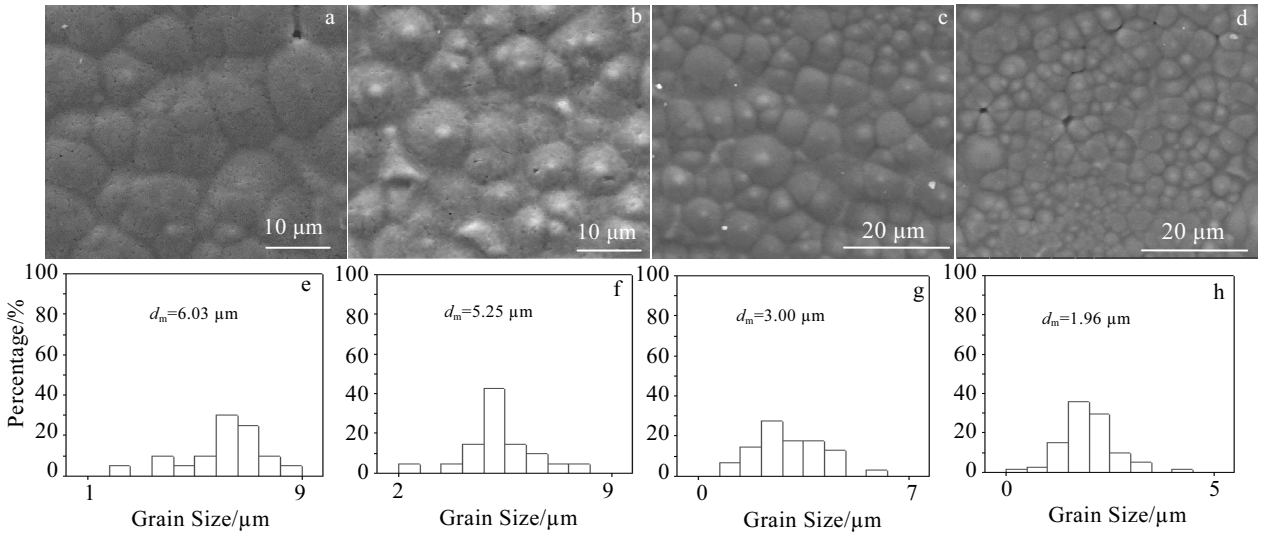

Fig.5 SEM images (a~d) and distribution of grain size (e~h)of ribbons at different wheel speeds (low magnification): (a, e) 12 m/s, (b, f) 18 m/s, (c, g) 24 m/s, and (d, h) 36 m/s

specific surface area. Meanwhile, due to the non-equilibrium rapid solidification and the existence of shear force between droplets and the roller, large quantities of defects (vacancy, dislocation, etc.) occur within the grains, and considerable quantity of suspension and unsaturated bonds are generated. The particle surface is in charged and the single grain exists unstably. According to the second law of thermodynamics, small particles agglomerate with the neighbor particles to reduce the surface free energy to reach a stable state. The size of agglomerated particles declines with the increase of quenching speed (under-cooling degree).

SEM images of ribbons at the speed of 18, 24 and 36 m/s are shown in Fig.6a~6c. With the increase of wheel speed, the grain size declines, and the uniformity is improved. The grain size ranges from 166 to 1300 nm ($d_m \approx$540 nm) when the speed is increased to 18 m/s, and declines to 166~878 nm ($d_m \approx$430 nm) when the wheel speed reaches 24 m/s.

The size decreases to 89~455 nm (d_m≈340 nm) at the speed of 36 m/s.

The melt-spun process belongs to non-equilibrium rapid solidification. Molten alloy contacts with the surface of cooling copper directly, resulting in a large temperature gradient and quick thermal transmission. Under-cooling degree, nucleation rate and grain growth rate increase with increase the wheel speed. According to the Newton's law of viscosity, the existence of shear stress before complete solidification causes numerous defects and nucleation positions. Therefore, the nucleation rate is higher than the growth rate in deep under-cooling. The higher wheel speed accelerates the thermal transmission significantly. The long-range diffusion of atoms is restrained in the solid-liquid interface, resulting in significant grain refinement (even less than 100 nm) and microstructure uniformity. Unfortunately, the grain size is restricted to submicron grade even if the speed is up to 45 m/s in Sm-Fe binary alloy, which can be improved by increasing the kind of alloy elements.

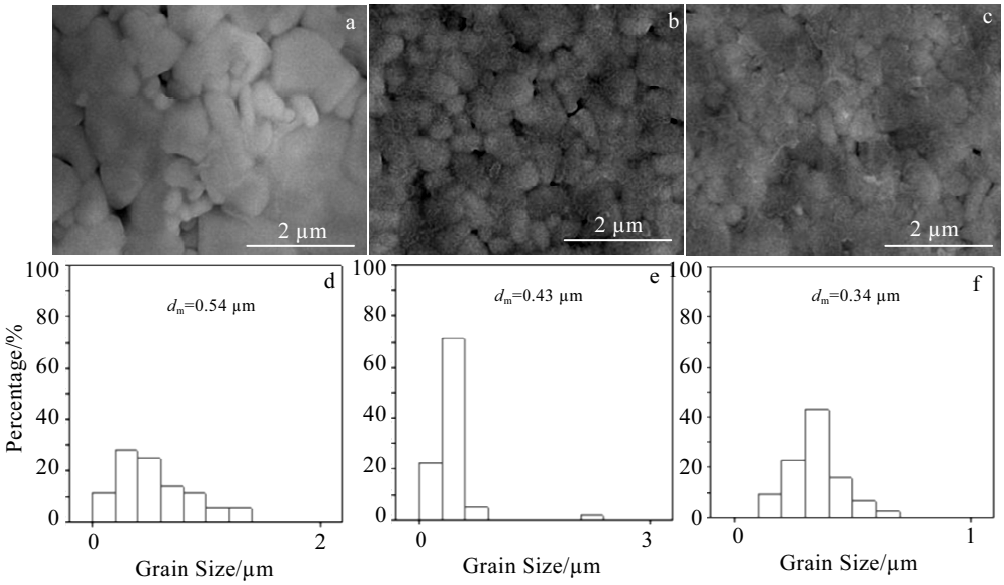

Fig.6 SEM images (a~c) and grain size distribution (d~f) of ribbons at different wheel speeds (high magnification): (a, d) 18 m/s, (b, e) 24 m/s, and (c, f) 36 m/s

To clarify the phase structure in melt-spun ribbons, XRD patterns of ribbons produced with different rates (24, 36, and 45 m/s) are shown in Fig.7. There exist three phases in the ribbons, Sm_2Fe_{17}, α-Fe and Sm-rich phase. The diffraction peaks (300), (220), (303), (024) and (303) of Sm_2Fe_{17} phase correspond to the 2θ angles ~ 36º, ~ 42.3º, ~ 42.6º and ~ 43.7º, respectively, the diffraction peak (110) of α-Fe corresponds to 2θ angles ~ 44.6º, and a certain amount of Sm-rich phase occurs at ~ 40.3º. The diffraction peak intensity of Sm_2Fe_{17} phase and bcc-Fe phase (110) enhances when increasing the wheel speed, and Sm-rich phase disappears for the volatilization of Sm element when increasing the wheel speed. Therefore, the characteristic peak intensity of $I_{(303)}/I_{(110)}$ enhances, indicating that the volume fraction of α-Fe phase increases. The superstructure peaks (024), which is used to distinguish the Sm_2Fe_{17} and $SmFe_9$ phases, disappears gradually with an increase of wheel speed. Therefore, the metastable $SmFe_9$ phase with a $TbCu_7$-type structure is formed at the speed of 45 m/s. One reason is the decrease of Sm content, and the other reason is that the rapid cooling rate promotes the formation of metastable phase. Fig.8 presents the partial XRD patterns of Fig.7. We can see that the diffraction peaks shift to the left and broaden with the increase of the wheel speed. These changes indicate the grains are refined, and lattice distortion enhances. The characteristic peak intensity of $I_{(303)}/ I_{(220)}$ enhances, the grains are of preferred orientation to some extent.

From the analysis of XRD, it can be concluded that Sm_2Fe_{17}, α-Fe and Sm-rich phase co-exist in the ribbons. The results are further confirmed by the BSE images (Fig.9a) and EDS spectrum (Fig.9c and Fig.9d). Table 1 shows the composition at different positions in Fig.9b. The α-Fe (dark) and Sm-rich phase (bright) are distributed around Sm_2Fe_{17} phase (gray). The Sm_2Fe_{17} phase shows an explosive nucleation, Sm-rich phase forms at grain boundaries and the residual Fe elements are precipitated around the Sm-rich phase in the form of α-Fe phase, due to the peritectic reaction. The partial oxidation of Sm-rich phase is inevitable, which must be controlled strictly to ensure the excellent magnetic properties.

Fig.10 presents the phase morphology and Sm distribution in melt-spun ribbons. The Sm-rich phase is distributed at Sm_2Fe_{17} grain boundary (Fig.10a), presenting two forms:

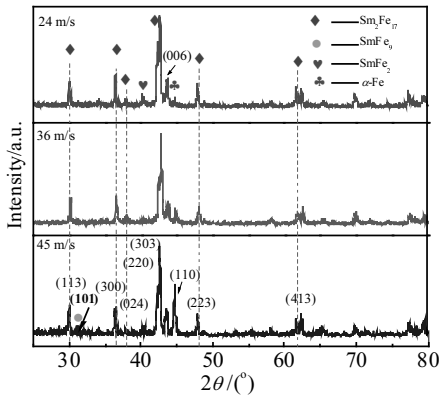

Fig.7 XRD patterns of Sm-Fe alloys at different wheel speeds

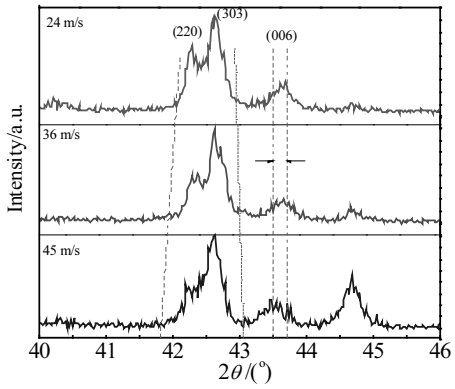

Fig.8 Partial XRD patterns of Sm-Fe alloys at different wheel speeds

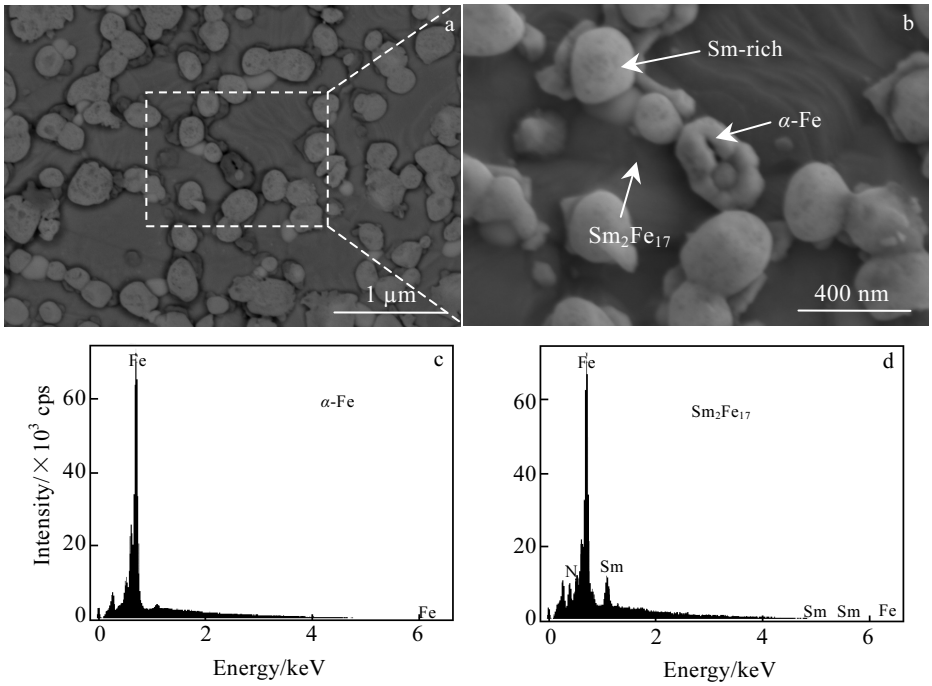

Fig.9 Morphologies and EDS analysis of phases distribution in ribbons: (a) BSE image; (b) SEM magnification image; (c) EDS spectrum of α-Fe; (d) EDS spectrum of Sm_2Fe_{17}

Table 1 EDS composition of various phases for SmFe alloy ribbons in Fig.9b (wt%)

Region	Sm	Fe
Bright (Sm-rich)	57.23	42.77
Gray (Sm_2Fe_{17})	24.02	75.98
Dark (α-Fe)	0	100

spherical and irregular (Fig.10b). Spherical grains exist in the center and irregular-shape at edges. Due to the energy difference at the grain boundaries, the spherical grains distribute around the smaller Sm_2Fe_{17} grains. The higher interface energy of the smaller Sm_2Fe_{17} grains and surface tension of the Sm-rich grains promote their spheroidization, and they are not higher enough to the bigger Sm_2Fe_{17} grains. Therefore irregular-shape grains are formed.

Different characterization methods were adopted to confirm the grain size. For the polished and etched specimen, the Sm-rich phase (white in BSE image) is distributed around the Sm_2Fe_{17} phases (Fig.11a). The grain size of Sm_2Fe_{17} phase, measured by the three methods, is in the same range (Fig.11 a~11c), which agrees well with the results in Fig.6.

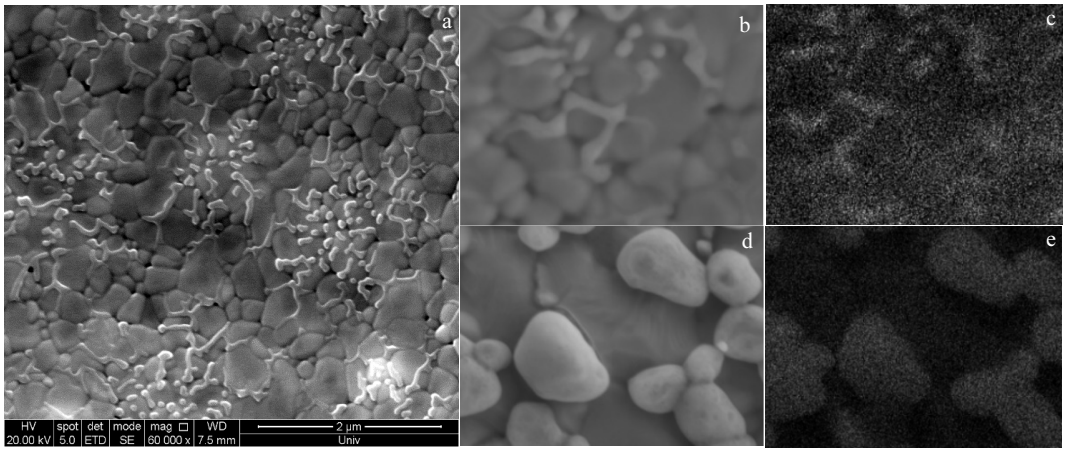

Fig.10 Morphologies of grain boundary phase in Sm-Fe alloy ribbons: (a) 60000×; (b, d) 100000×; (c, e) EDS mapping of Sm element

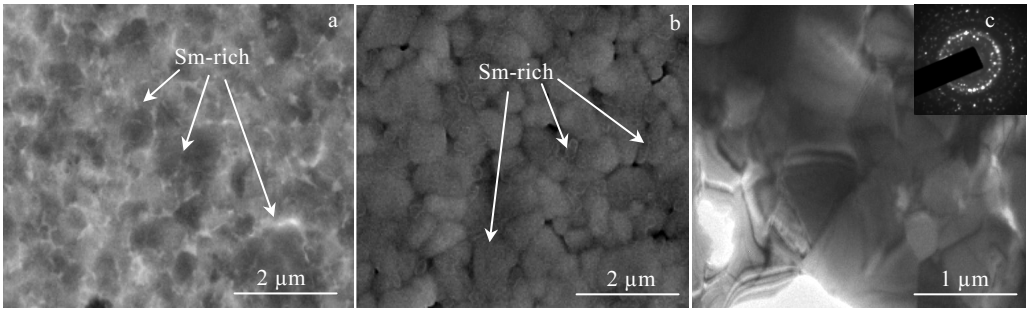

Fig.11 Grain morphologies with different characterization methods (24 m/s): (a) BSE image after polished and etched specimen; (b) SEM image of surface without polishing and corrosion; (c) TEM image and SAED pattern

3 Conclusions

1) The thickness of Sm-Fe alloy ribbons declines from 34 μm (12 m/s) to 19 μm (45 m/s) when increasing the wheel speed from 12 m/s to 36 m/s, but it is difficult to further decline.

2) Melt-spun ribbon mainly consists of Sm_2Fe_{17} phase, α-Fe phase and Sm-rich phase, and $SmFe_9$ metastable phase occurs when the wheel speed increases to 45 m/s, which can be proved by the disappearance of (024) diffraction peak.

3) All the diffraction peaks shift to the left and broaden with increase the wheel speeds, indicating that the grains are refined, and the lattice distortion enhances. The characteristic peak intensity of $I_{(303)}/I_{(220)}$ enhances, and the grains are of preferred orientation to some extent.

4) When the wheel speed increases to 45 m/s, the main grain size is merely in submicron grade, ~340 nm, and further refinement is difficult to obtain only by increasing wheel speed.

References

1 Coey J M D, Sun H. *J Magn Magn Mater*[J], 1990, 87(3): L251
2 Bernardi J, Schrefl T, Fidler J *et al*. *J Magn Magn Mater*[J], 2000, 219(2): 186
3 Sugimoto S. *J Phys D: Appl Phys*[J], 2011, 44(6): 064 001
4 Li Y P, Wang F Q, Liu J P *et al*. *J Magn Magn Mater*[J], 2020, 498: 166191
5 Pandey T, Du M H, Parker D S. *Phys Rev Appl*[J], 2018, 9(3): 034 002
6 Dirba I, Sepehri-Amin H, Ohkubo T *et al*. *Acta Mater*[J], 2019, 165: 373
7 Wuest H, Bommer L, Huber A M *et al*. *J Magn Magn Mater*[J], 2017, 428: 194
8 Lv B B Yu D B, Zhang S R *et al*. *J Rare Earths*[J], 2013, 31(10): 979
9 Luo Y, Yu D B, Li H W *et al*. *J Rare Earths*[J], 2013, 31(4): 381
10 Wu G, Li H, Yu D *et al*. *J Rare Earths*[J], 2018, 36(3): 281
11 Pandey T, Du M H, Parker D S. *Phys Rev Appl*[J], 2018, 9(3): 034 002
12 Tarasov V P, Ignatov A S, Kutepov D A. *Mater Metallurgist*[J], 2017, 60(11-12): 1183
13 Yasuhara A, Park H S, Shindo D *et al*. *J Magn Magn Mater*[J], 2005, 295(1): 1
14 Saito T, Nishio-Hamane D. *AIP Adv*[J], 2018, 8(5): 056 230
15 Kobayashi K, Furusawa D, Suzuki S *et al*. *Mater Trans*[J], 2018, 59(11): 1845
16 Lu C, Hong X, Bao X *et al*. *J Alloy Compd*[J], 2019, 784: 980

17 Hirayama Y, Panda A K, Ohkubo T *et al*. *Scr Mater*[J], 2016, 120: 27
18 Okada S, Suzuki K, Node E *et al*. *J Alloy Compd*[J], 2017, 695: 1617
19 Ye J W, Liu Y, Li M *et al*. *Rare Metals*[J], 2006, 25(6): 568
20 Sellmyer D J. *Nature*[J], 2002, 420(6914): 374
21 Xiao X F, Si P Z, Ge H L *et al*. *J Electron Mater*[J], 2018, 47(12): 7472
22 Chen X X, Luo Y, Hu Z *et al*. *Rare Metals*[J], 2017, 36(1): 1

Sm_2Fe_{17} 快淬薄带形貌及相组成的分析研究

柳　昆[1]，王书桓[1,2]，冯运莉[1]，张一昆[1]
(1. 华北理工大学 冶金与能源学院，河北 唐山 063210)
(2. 唐山市特种冶金及材料制备重点实验室，河北 唐山 063210)

摘　要：采用 X 射线衍射（XRD）、光学显微镜（OM）、扫描电子显微镜（SEM）和高分辨率透射电子显微镜（HRTEM）分析了快淬速度对 Sm-Fe 合金带相组成和形貌的影响，并结合了 3 种不同的方法对 Sm_2Fe_{17} 薄带及微观组织进行了表征。结果表明：随着辊速的增加，合金薄带的尺寸在宽度和厚度方向上逐渐减小，当速度连续增加时，合金带的尺寸在厚度方向上趋于稳定。当辊速提高到 36 m/s 时，薄带自由表面中团聚体态颗粒尺寸减小，为 0.5~3 μm。XRD 和 EDS 结果均表明，薄带中存在 3 种相分别为：Sm_2Fe_{17}、α-Fe 相和富 Sm 相。Sm_2Fe_{17} 相的晶粒尺寸为亚微米级（d_m≈340 nm，36 m/s），这是辊速与元素种类共同限制的结果。

关键词：晶粒形貌；辊速；晶粒团聚；Sm-Fe合金

作者简介：柳 昆，女，1988 年生，博士，华北理工大学冶金与能源学院，河北 唐山 063210，E-mail: 79890799@qq.com